© 2017. Published by The Company of Biologists Ltd | Development (2017) 144, 2165-2174 doi:10.1242/dev.149518

RESEARCH ARTICLE

Histone acetyltransferase KAT8 is essential for mouse oocyte development by regulating reactive oxygen species levels

Shi Yin[1,*], Xiaohua Jiang[1,*], Hanwei Jiang[1], Qian Gao[1], Fang Wang[1], Suixing Fan[1], Teka Khan[1], Nazish Jabeen[1], Manan Khan[1], Asim Ali[1], Peng Xu[2], Tej K. Pandita[3], Heng-Yu Fan[4], Yuanwei Zhang[1] and Qinghua Shi[1,‡]

ABSTRACT

Proper oocyte development is crucial for female fertility and requires timely and accurate control of gene expression. K (lysine) acetyltransferase 8 (KAT8), an important component of the X chromosome dosage compensation system in *Drosophila*, regulates gene activity by acetylating histone H4 preferentially at lysine 16. To explore the function of KAT8 during mouse oocyte development, we crossed *Kat8*$^{flox/flox}$ mice with *Gdf9-Cre* mice to specifically delete *Kat8* in oocytes. Oocyte *Kat8* deletion resulted in female infertility, with follicle development failure in the secondary and preantral follicle stages. RNA-seq analysis revealed that *Kat8* deficiency in oocytes results in significant downregulation of antioxidant genes, with a consequent increase in reactive oxygen species. Intraperitoneal injection of the antioxidant N-acetylcysteine rescued defective follicle and oocyte development resulting from *Kat8* deficiency. Chromatin immunoprecipitation assays indicated that KAT8 regulates antioxidant gene expression by direct binding to promoter regions. Taken together, our findings demonstrate that KAT8 is essential for female fertility by regulating antioxidant gene expression and identify KAT8 as the first histone acetyltransferase with an essential function in oogenesis.

KEY WORDS: *Kat8*, H4K16ac, Oocyte, Follicle, Sterility, ROS

INTRODUCTION

Oogenesis plays a key role in female fertility as it determines the production of healthy eggs (Rodrigues et al., 2008). Oocyte growth, which is accompanied by follicle development, is an important part of oogenesis. In mice, oocyte growth begins from 5 days postpartum and continues to the full-grown germinal vesicle (GV) stage (Lucifero et al., 2007). During this period, the oocyte grows rapidly in size and is transcriptionally active (Jagarlamudi and Rajkovic, 2012), which is essential for the oocyte to achieve further development and final maturation (van den Hurk and Zhao, 2005).

To ensure the normal growth of oocytes, excessive apoptosis must be avoided by promoting the expression of anti-apoptotic genes. Several factors can induce oocyte apoptosis in mammals, such as increased levels of reactive oxygen species (ROS) or destruction of oocyte-granulosa cell communication (Tiwari et al., 2015). However, how anti-apoptotic genes are regulated in response to these apoptosis inducers is still not fully understood.

In oocytes, transcriptional activity is associated with histone modifications, including acetylation (Gu et al., 2010). The level of histone acetylation is controlled by the opposing activity of histone acetyltransferases (HATs) and histone deacetylases (HDACs) (Ma et al., 2012). HATs, which comprise the MYST, Gcn5/PCAF and p300/CBP subfamilies (Gu et al., 2010), add acetyl groups to histone lysines, which weakens the electrostatic affinity between histones and DNA, resulting in an open chromatin structure that promotes transcription factor binding and thus gene activity. By contrast, HDACs mainly repress transcription by removing acetyl groups from histone lysine residues, which results in a more compact chromatin structure (Shahbazian and Grunstein, 2007). Among the multiple acetylatable lysines (K), the deacetylation of H4 at lysine 16 has been found to be essential for mouse oocyte maturation. Depletion of the HDACs HDAC2 or SIRT6 in oocytes within primary or antral follicles results in increased H4K16ac levels in metaphase II (MII) oocytes (Han et al., 2015; Ma and Schultz, 2013), decreases the number of antral follicles (Ma and Schultz, 2013) and causes defects in spindle assembly and chromosome segregation in MII oocytes (Han et al., 2015; Ma and Schultz, 2013). Although a high level of H4K16ac is observed in GV stage oocyte (Pan et al., 2012), whether it is necessary for oogenesis is unknown.

K (lysine) acetyltransferase 8 (KAT8, also known as MOF or MYST1) is a highly conserved MYST family member specifically responsible for H4K16 acetylation (Gupta et al., 2013). KAT8 contains a chromodomain for DNA binding and a C-terminal HAT domain for histone acetylation (Su et al., 2016). It is expressed in most tissues, including the ovary (Thomas et al., 2007), and affects gene expression in multiple biological processes. *Drosophila* MOF is essential for dosage compensation in males by inducing a 2-fold transcriptional upregulation of X-linked genes (Akhtar and Becker, 2000). In mouse embryonic stem cells (ESCs), *Kat8* is necessary for the maintenance of self-renewal and pluripotency by promoting the expression of key transcription factors (Li et al., 2012). Although oocyte development is associated with dramatic changes in gene expression, whether KAT8 functions in this process is unknown.

Here, we specifically deleted *Kat8* in mouse oocytes. The conditional knockout females were sterile, with defective oocyte and follicle development. Our findings identify KAT8 as the first HAT with an essential role in mouse follicle development and female fertility.

[1]Molecular and Cell Genetics Laboratory, The CAS Key Laboratory of Innate Immunity and Chronic Diseases, Hefei National Laboratory for Physical Sciences at Microscale, School of Life Sciences, CAS Center for Excellence in Molecular Cell Science, University of Science and Technology of China, Collaborative Innovation Center of Genetics and Development, Collaborative Innovation Center for Cancer Medicine, Hefei, Anhui 230027, China. [2]USTC-Shenyang Jinghua Hospital Joint Center of Human Reproduction and Genetics, Shenyang, Liaoning 110000, China. [3]Department of Radiation Oncology, Houston Methodist Research Institute, Houston, TX 75390, USA. [4]Life Sciences Institute, Zhejiang University, Hangzhou, Zhejiang 310058, China.
*These authors contributed equally to this work

‡Author for correspondence (qshi@ustc.edu.cn)

S.Y., 0000-0001-7730-633X; X.J., 0000-0002-5682-6827; H.J., 0000-0001-8640-7714; P.X., 0000-0001-7405-9388

Received 25 January 2017; Accepted 29 April 2017

Development (2017) 144, 2165-2174 doi:10.1242/dev.149518

RESULTS

Kat8 expression in oocytes and granulosa cells

To explore the role of *Kat8* during follicle development, we first examined gene expression in ovarian cells of wild-type (WT) mice. Analysis of *Kat8* mRNA levels in oocytes and granulosa cells from antral follicles by RT-PCR revealed that both cell types express *Kat8* (Fig. 1A), with much higher expression levels in oocytes than in granulosa cells. We next analyzed *Kat8* expression during oocyte development and detected a dramatic increase (~5-fold) between 14 days and full-grown GV stage oocytes, followed by a sharp decrease (2.3% to GV stage) in germinal vesicle breakdown (GVBD)-metaphase I (MI) stage oocytes (Fig. 1B). Immunostaining revealed that KAT8 protein is mainly located in the nucleus throughout the growth phase, but upon GVBD the staining intensity decreased and the signal became uniformly dispersed throughout the oocyte (Fig. 1C).

Given that *Kat8* is essential for histone modification, we also analyzed H4K16 acetylation levels, the major histone target of KAT8, in oocytes at different developmental stages. Immunocytochemical assays showed that, consistent with the KAT8 localization profile, nuclear staining of H4K16ac increased from 14 days to GV stage and decreased significantly upon GVBD (Fig. S1).

Specific *Kat8* deletion in oocytes leads to abnormal oogenesis and female sterility

To study the role of *Kat8* during oocyte development, we generated mice in which *Kat8* was specifically disrupted in oocytes. We crossed female *Kat8*$^{flox/flox}$ mice, which have loxP sites flanking exons 1 to 3 of *Kat8* (Gupta et al., 2008; Kumar et al., 2011), with *Gdf9-Cre* males. Expression of Cre recombinase begins in mouse oocytes at 3 days (Lan et al., 2004). Real-time PCR and western blot confirmed that oocytes from *Gdf9-Cre; Kat8*$^{flox/flox}$ (referred to as *Kat8*^{Gdf9} cKO) mice had negligible expression of *Kat8* mRNA and protein (Fig. 2A,B), confirming efficient deletion of *Kat8*. Additionally, *Kat8* deletion resulted in a decrease in H4K16ac without affecting acetylation at other detected histone residues in oocytes (Fig. S2).

To determine their fertility, *Kat8*^{Gdf9} cKO females and WT controls were bred to WT males for 6 months. A total of 312 pups were produced from eight WT females, whereas no offspring were born to the eight *Kat8*^{Gdf9} cKO females (Fig. 2C). Compared with WT mice, 8-week-old *Kat8*^{Gdf9} cKO females had substantially smaller ovaries (Fig. 2D) and a 77.4% lower ovary to body weight ratio (Fig. 2E). Following pregnant mare serum gonadotropin (PMSG) priming, ~50 full-grown GV stage oocytes were recovered from each WT female, but only ~20 oocytes from each *Kat8*^{Gdf9} cKO mouse (Fig. 2G). Notably, *Kat8*^{Gdf9} cKO oocytes were much smaller than WT oocytes (mean diameter 63.7 µm versus 81.4 µm, respectively; Fig. 2H), and exhibited abnormal morphology, including cytoplasmic granulation, shrinkage and an irregular shape (Fig. 2F). Together, these results indicate that *Kat8* is essential for fertility and oogenesis.

Kat8^{Gdf9} cKO females display defects in follicle development and increased oocyte apoptosis

To investigate how *Kat8* deletion disrupts oogenesis, we carefully analyzed follicle development in *Kat8*^{Gdf9} cKO females. Ovaries from 2-week-old *Kat8*^{Gdf9} cKO mice were indistinguishable from WT ovaries in morphology and contained comparable numbers of

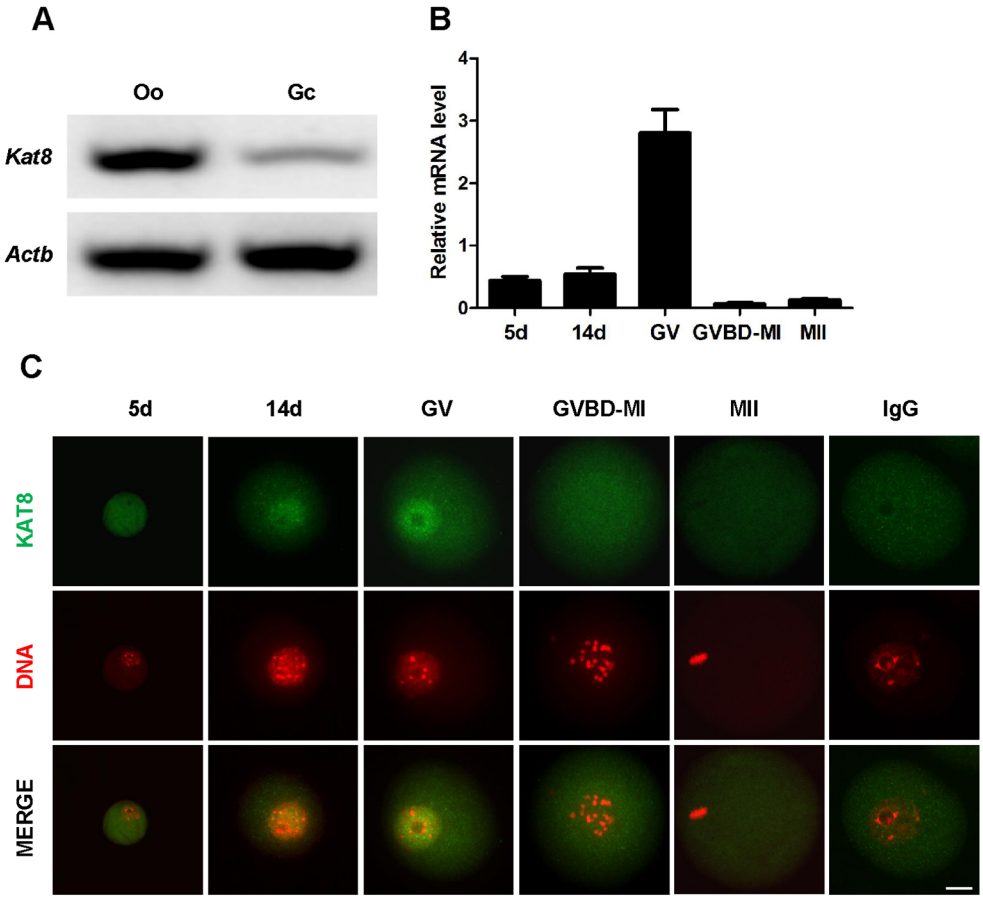

Fig. 1. *Kat8* expression in oocytes and granulosa cells. (A) RT-PCR analysis of *Kat8* mRNA levels in oocytes (Oo) and granulosa cells (Gc) from antral follicles of WT mice. (B) *Kat8* expression during oocyte development. *Kat8* mRNA levels in oocytes at different growth phases were determined by real-time PCR, and normalized to *Actb*. 5 d, 5 days postpartum; 14 d, 14 days postpartum; GV, full-grown germinal vesicle; GVBD, germinal vesicle breakdown; MI, metaphase I; MII, metaphase II. Data are mean±s.e.m. from three independent experiments. (C) KAT8 immunostaining of oocytes at different growth phases. IgG was used as a negative control. Scale bar: 20 µm. Images (A,C) are representative of three independent experiments.

Development (2017) 144, 2165-2174 doi:10.1242/dev.149518

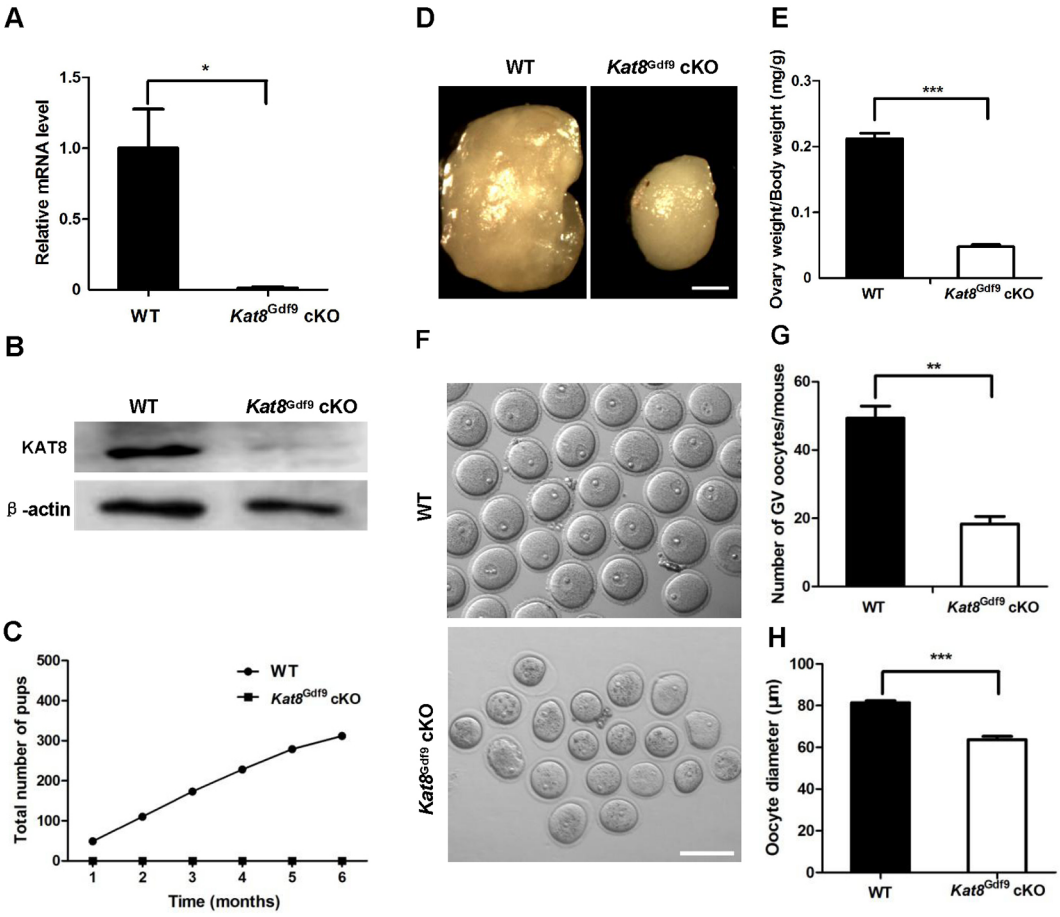

Fig. 2. *Kat8*^{Gdf9} cKO mice display abnormal oogenesis and sterility. (A) Real-time PCR analysis of *Kat8* mRNA levels in oocytes from 2-week-old WT and *Kat8*^{Gdf9} cKO mice. *Kat8* mRNA levels in WT oocytes were arbitrarily set to 1, and values were normalized and plotted against *Actb*. (B) Western blot analysis of KAT8 in oocytes from 2-week-old mice. Per sample, ∼200 oocytes were used; β-actin served as a protein loading control. Images shown are representative of three independent experiments. (C) Fertility test. The cumulative number of pups obtained from matings of eight WT and eight *Kat8*^{Gdf9} cKO females to WT males over a 6 month period. (D) Representative images of ovaries from 8-week-old females. Scale bar: 0.5 mm. (E) Ratio of ovary weight to body weight in 8-week-old mice. (F) Representative images of GV stage oocytes from 8-week-old mice. Scale bar: 200 µm. (G) Mean number of GV stage oocytes obtained per mouse after priming with PMSG. (H) Mean diameter of GV stage oocytes. (A,E,G,H) Data are mean±s.e.m. from three independent experiments. **P*<0.05, ***P*<0.01, ****P*<0.001, *t*-test.

follicles at different developmental stages (Fig. 3A,B). However, *Kat8*^{Gdf9} cKO ovaries from 3-week-old females contained 50.4%, 49.6% and 78.7% fewer secondary, preantral and antral follicles, respectively, than WT ovaries, but 2-fold more atretic follicles (Fig. 3A,B).

The defective oogenesis and follicle development in *Kat8*^{Gdf9} cKO females strongly implied that *Kat8*-deficient oocytes undergo apoptosis. To confirm this, we performed terminal deoxynucleotidyl transferase dUTP nick end labeling (TUNEL) assays in oocytes isolated from 3-week-old females (oocyte diameter of 50-70 µm, mainly from secondary and preantral follicles) (Monti and Redi, 2009). Indeed, *Kat8*^{Gdf9} cKO oocytes exhibited a significantly higher incidence of apoptosis than WT oocytes (∼17.2% versus ∼5.7%; Fig. 3C,D). As DNA damage is a major trigger of cell apoptosis (Ma et al., 2013), we measured DNA double-strand breaks (DSBs) in oocytes by immunostaining for phosphorylated histone H2AX (γ-H2AX), a commonly used surrogate marker for DSBs. The ratio of oocytes with more than five γ-H2AX foci (Fig. 3E,F) was significantly increased in *Kat8*^{Gdf9} cKO (∼56.8%) compared with WT (∼14.6%) oocytes. TUNEL assay and γ-H2AX immunostaining performed on ovary sections confirmed that oocytes undergoing apoptosis or exhibiting severe DNA damage were localized in secondary and preantral follicles, but not in primordial or primary follicles (Fig. S3). Additionally, we found that *Kat8* deletion in oocytes did not affect the proliferation of granulosa cells, as confirmed by bromodeoxyuridine (BrdU) incorporation and PCNA immunostaining (Fig. S4A,B). Also, expression levels of the oocyte factors *Gdf9* and *Bmp15* (McNatty et al., 2005) did not differ significantly between WT and *Kat8*^{Gdf9} cKO oocytes (Fig. S4C). Taken together, these results indicate that *Kat8* is essential for follicle development by maintaining oocyte survival.

Kat8^{Gdf9} cKO oocytes exhibit decreased antioxidant gene expression and excess ROS levels

To explore the mechanism of *Kat8*-dependent oogenesis and folliculogenesis, we performed whole-transcriptome sequencing (RNA-seq) on oocytes (50-70 µm diameter) from 2-week-old mice. Accuracy of the sequencing data was validated by real-time PCR of mRNA levels for randomly selected genes. Consistent expression trends from both real-time PCR and RNA-seq for all eight selected test genes confirmed reliability of the sequencing data (Fig. S5A). Data analysis identified 858 significant differentially expressed genes, 500 of which were upregulated and 358 downregulated in *Kat8*^{Gdf9} cKO oocytes (Tables S3 and S4, Fig. S5B).

Development (2017) 144, 2165-2174 doi:10.1242/dev.149518

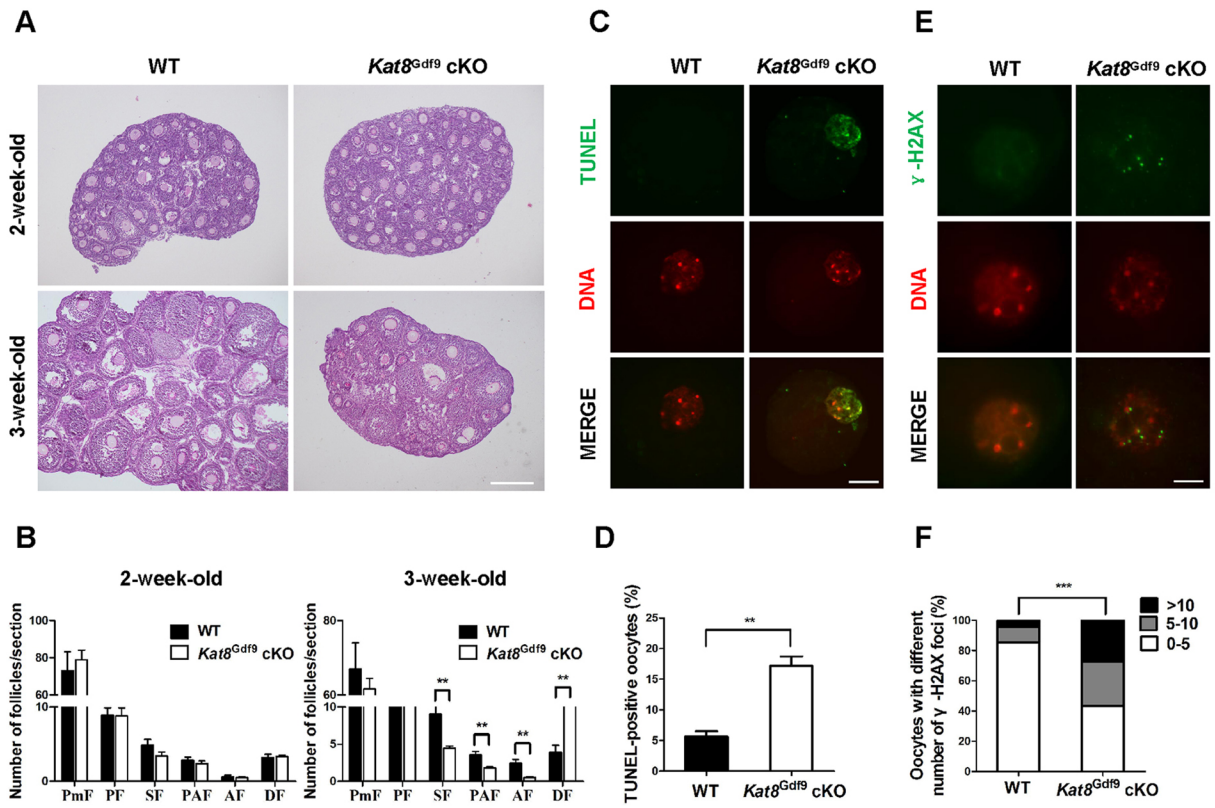

Fig. 3. *Kat8* deletion in oocytes causes follicle loss and oocyte defects. (A) Histological sections of ovaries from 2- and 3-week-old females stained with Hematoxylin and periodic acid-Schiff (PAS) reagent. (B) Quantitative analysis of follicles at different stages in ovary sections from 2- and 3-week-old WT and *Kat8*^{Gdf9} cKO females. PmF, primordial follicles; PF, primary follicles; SF, secondary follicles; PAF, preantral follicles; AF, antral follicles; DF, degenerating follicles. (C) Detection of apoptosis by TUNEL assay in oocytes from 3-week-old mice. (D) Percentage of TUNEL-positive oocytes. (B,D) Data are mean±s.e.m. from three independent experiments. $^{**}P$<0.01, *t*-test. (E) Visualization of DSBs in oocyte nuclei from 3-week-old mice by γ-H2AX staining. (F) Proportions of WT and *Kat8*^{Gdf9} cKO oocytes with various numbers of γ-H2AX foci per nucleus. $^{***}P$<0.001, Chi-square test. Images (A,C,E) are representative of three independent experiments. Scale bars: 200 µm in A; 20 µm in C; 10 µm in E.

Gene Ontology (GO) enrichment analysis of the differentially expressed genes identified the term 'oxidation-reduction process' among the most enriched downregulated biological processes (Fig. S5C). Continuous scavenging of ROS by antioxidant enzymes represents one cellular mechanism of defense against oxidative damage, which may compromise DNA integrity and cause oocyte apoptosis (Devine et al., 2012). Among the differently expressed genes after *Kat8* deletion, the antioxidant genes peroxiredoxin 1 and 2 (*Prdx1*, *Prdx2*) and glutathione peroxidase 1 and 4 (*Gpx1*, *Gpx4*) were significantly downregulated in *Kat8*^{Gdf9} cKO oocytes (Table S4), which was confirmed by real-time PCR (Fig. 4A). As these genes are responsible for reducing endogenous oxidative stress (Brigelius-Flohé and Maiorino, 2013; Rhee, 2016), we evaluated oocyte ROS levels by measuring the fluorescence of 5(6)-carboxy-2′7′-dichlorofluorescein (carboxy-DCF), a fluorescent dye oxidized by ROS. Oocytes lacking *Kat8* exhibited a greater than 2-fold increase in ROS compared with WT oocytes (Fig. 4B,C). These results demonstrate that *Kat8*^{Gdf9} cKO oocytes display decreased antioxidant gene expression and a corresponding increase in ROS levels.

N-acetylcysteine treatment rescues the *Kat8* null phenotype

To further confirm that excessive ROS levels resulting from decreased expression of antioxidant genes caused the defective follicle development and increased oocyte apoptosis in *Kat8*^{Gdf9} cKO females, we performed a rescue experiment by supplying an exogenous antioxidant. N-acetylcysteine (NAC) is a precursor of intracellular cysteine and reduced glutathione and a proven potent antioxidant in various tissue types (Danilovic et al., 2011; Inci et al., 2007; Usta et al., 2008). Following intraperitoneal injection of 150 mg/kg NAC daily for 7 days, folliculogenesis in WT mice did not differ detectably from that of mice injected with PBS only (WT+PBS; data not shown). By contrast, *Kat8*^{Gdf9} cKO mice injected with NAC (*Kat8*^{Gdf9} cKO+NAC) had larger ovaries than PBS-injected *Kat8*^{Gdf9} cKO mice (*Kat8*^{Gdf9} cKO+PBS) (Fig. 5A,B). In addition, more MII oocytes were recovered from *Kat8*^{Gdf9} cKO+NAC mice than from *Kat8*^{Gdf9} cKO+PBS mice following gonadotropin injection (Fig. 5C,D). Histological analysis revealed significantly improved follicular development and survival in *Kat8*^{Gdf9} cKO mice following NAC injection. Compared with *Kat8*^{Gdf9} cKO+PBS ovaries, *Kat8*^{Gdf9} cKO+NAC ovaries exhibited a 60.0%, 83.8% and 224.2% increase in the number of secondary, preantral and antral follicles, respectively. Moreover, the number of atretic follicles in *Kat8*^{Gdf9} cKO+NAC groups decreased by 54.7% compared with that in *Kat8*^{Gdf9} cKO+PBS females (Fig. 5E,F).

To confirm these rescue effects, we measured ROS levels, DSBs and apoptosis in *Kat8*^{Gdf9} cKO oocytes after NAC treatment. Fluorescence intensity analysis showed that ROS levels in *Kat8*^{Gdf9} cKO+NAC oocytes decreased by 67.1% compared with *Kat8*^{Gdf9} cKO+PBS oocytes (Fig. 6A,B). Furthermore, *Kat8*^{Gdf9} cKO+NAC oocytes exhibited significantly lower levels of DSBs and contained a significantly smaller proportion of TUNEL-positive oocytes, with

Development (2017) 144, 2165-2174 doi:10.1242/dev.149518

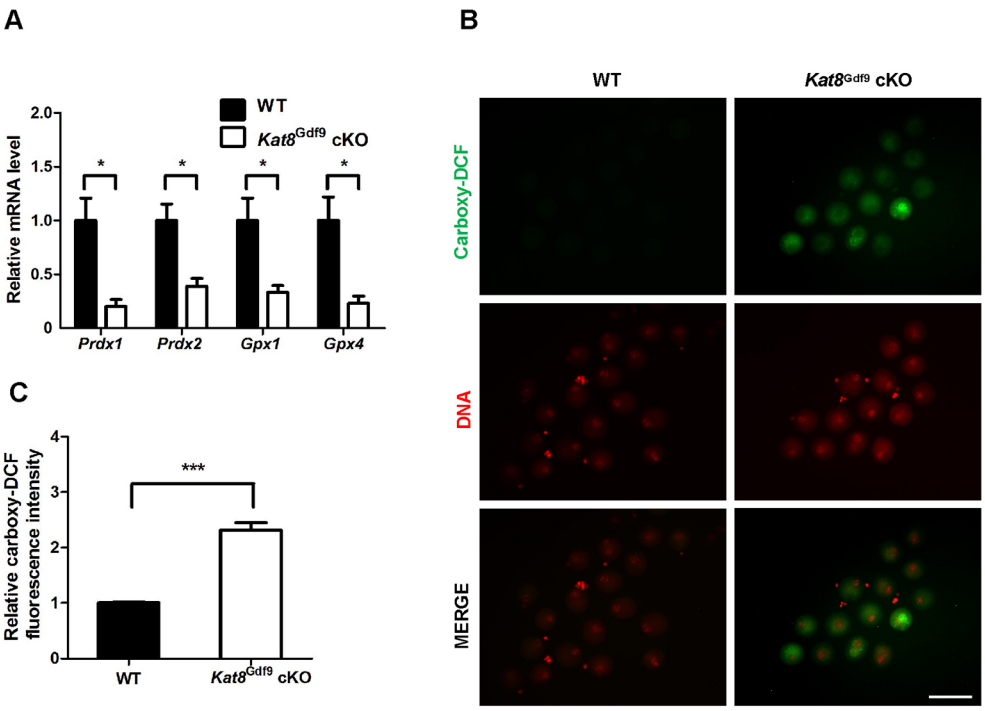

Fig. 4. Antioxidant gene expression decreases and ROS levels increase in *Kat8*^{Gdf9} cKO oocytes. (A) Relative mRNA levels of the antioxidant genes *Prdx1*, *Prdx2*, *Gpx1* and *Gpx4* in oocytes from 2-week-old WT and *Kat8*^{Gdf9} cKO females as detected by real-time PCR. The mRNA levels in WT oocytes were arbitrarily set to 1, and values were normalized to *Actb*. (B) Oocytes isolated from 2-week-old mice were treated with 5(6)-carboxy-2′7′-dichlorodihydrofluorescein diacetate (carboxy-H2DCFDA) for ROS detection. Images shown are representative of three independent experiments. Scale bar: 100 µm. (C) ROS levels in B were quantified by measuring carboxy-DCF fluorescence intensity. (A,C) Data are mean±s.e.m. from three independent experiments. *P<0.05, ***P<0.001, *t*-test.

58.7% and 56.1% reductions, respectively, compared with *Kat8*^{Gdf9} cKO+PBS oocytes (Fig. 6C-F). These results further confirm that excessive ROS levels are the direct cause of the defective follicle development and increased oocyte apoptosis in *Kat8*^{Gdf9} cKO females.

KAT8 directly regulates antioxidant gene expression in oocytes

To determine whether endogenous KAT8 directly regulates antioxidant gene expression, we performed chromatin immunoprecipitation (ChIP) analysis on oocytes from 2-week-old

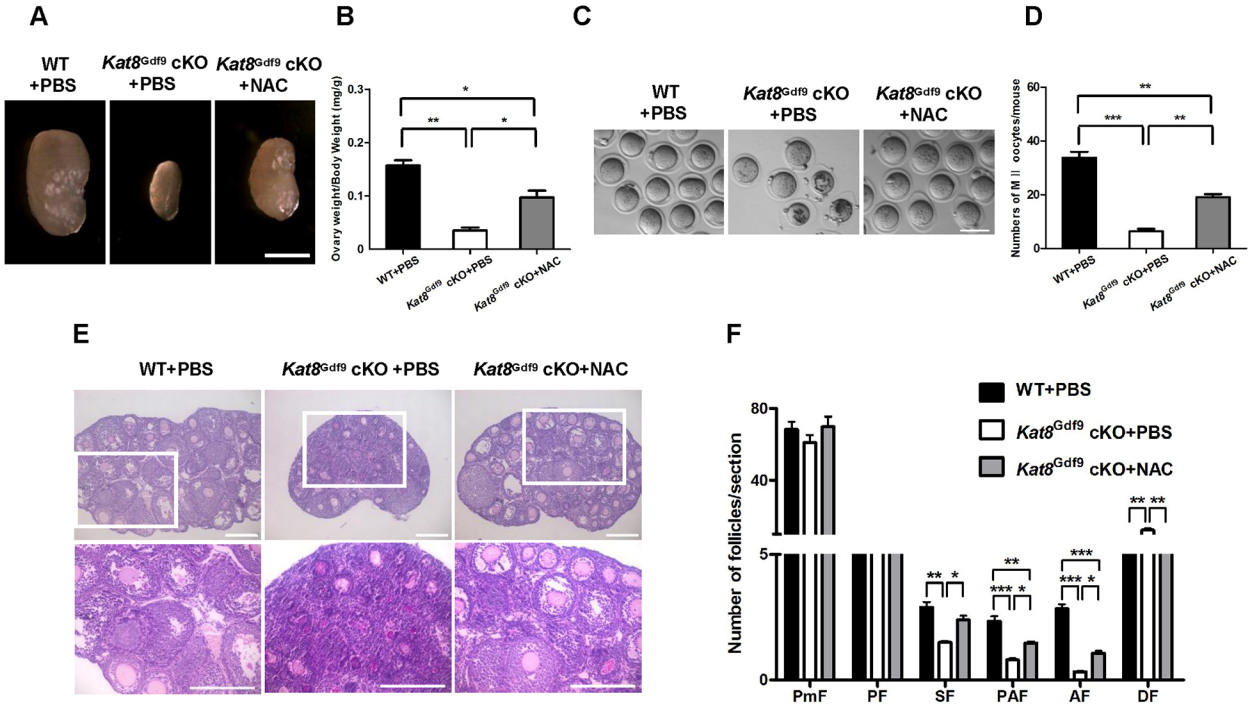

Fig. 5. NAC treatment partially rescues folliculogenesis in *Kat8*^{Gdf9} cKO females. (A) Ovaries from 3-week-old PBS- or NAC-treated mice. (B) Ratio of ovary weight to body weight in 3-week-old mice. (C) MII oocytes from 3-week-old mice. (D) Mean number of MII oocytes collected from each female following superovulation with PMSG and HCG. (E) Ovary sections from 3-week-old mice stained with Hematoxylin and PAS. Boxed regions are magnified beneath. (F) Quantitative analysis of follicles at different stages in ovary sections from PBS- or NAC-treated mice. (B,D,F) Data are mean±s.e.m. from three independent experiments. *P<0.05, **P<0.01, ***P<0.001, one-way ANOVA. Images (A,C,E) are representative of three independent experiments. Scale bars: 0.5 mm in A; 100 µm in C; 200 µm in E.

Development (2017) 144, 2165-2174 doi:10.1242/dev.149518

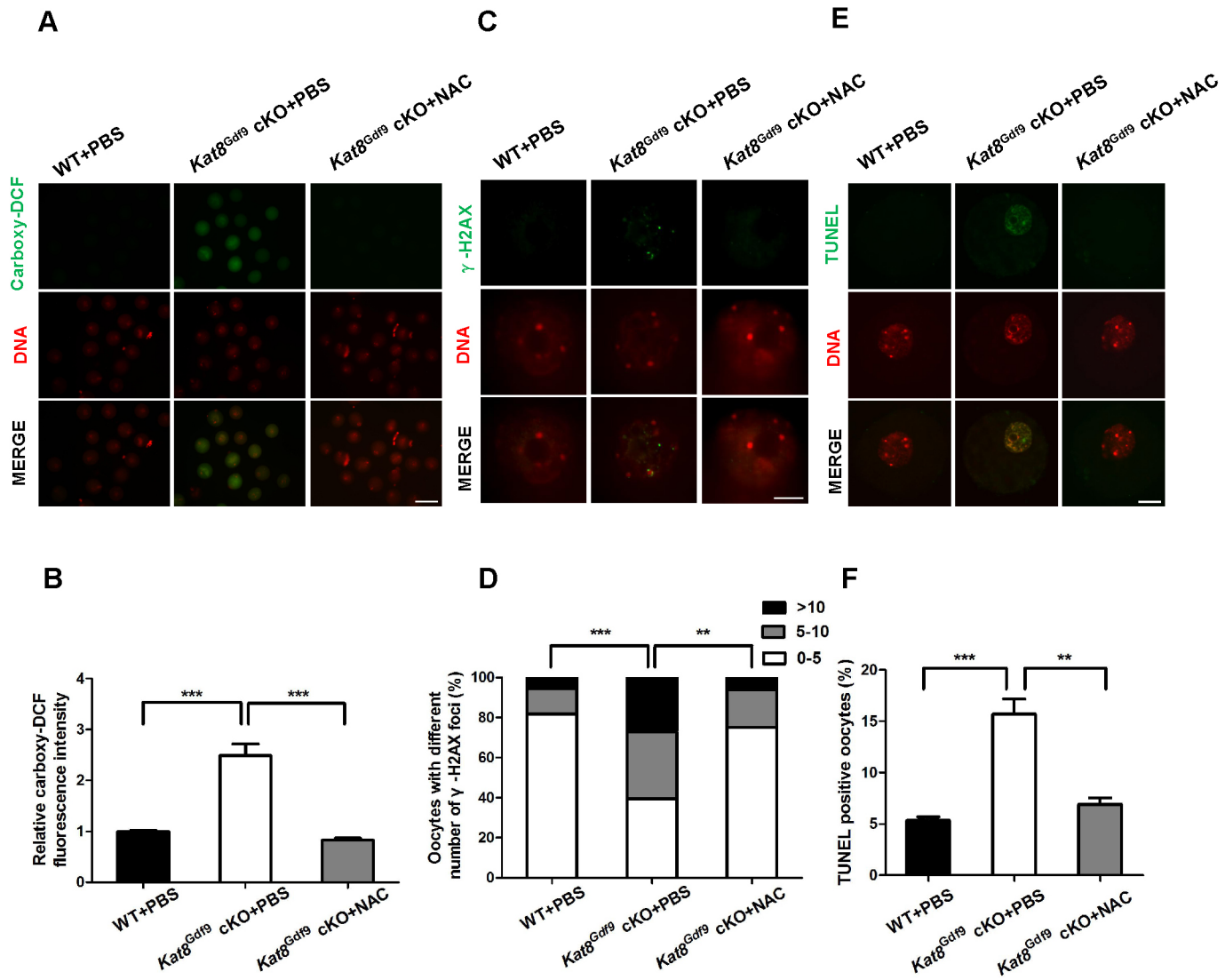

Fig. 6. Antioxidant treatment decreases ROS levels, DSBs and apoptosis in *Kat8*^{Gdf9} cKO oocytes. (A) Oocytes isolated from 3-week-old PBS- or NAC-injected mice were treated with carboxy-H2DCFDA for ROS detection. (B) ROS levels were quantified by measuring carboxy-H2DCFDA fluorescence intensity. (C) DSBs were detected by γ-H2AX staining in oocyte nuclei from 3-week-old PBS- or NAC-treated mice. (D) Proportions of oocytes containing various numbers of γ-H2AX foci. (E) Detection of apoptosis by TUNEL assay in oocytes from 3-week-old PBS- or NAC-treated mice by TUNEL assay. (F) Percentage of TUNEL-positive oocytes in 3-week-old PBS- or NAC-treated mice. Data (B,F) are mean±s.e.m. from three independent experiments. ***P*<0.01, ****P*<0.001, one-way ANOVA (B,F) or Chi-square test (D). Images (A,C,E) are representative of three independent experiments. Scale bars: 100 µm in A; 10 µm in C; 20 µm in E.

mice. We detected a greater than 4-fold enrichment of KAT8 at the *Prdx1*, *Gpx1* and *Gpx4* promoters. Given that KAT8 is essential for H4K16ac, we additionally performed H4K16ac ChIP and detected a greater than 9-fold enrichment at the *Gpx1* and *Gpx4* promoters (Fig. 7), which implies that KAT8 can regulate the expression of these genes either through regulation of H4K16ac or by direct binding to the promoters. These data, together with the transcriptome analysis, indicate that KAT8 plays an essential and direct role in mediating antioxidant gene transcription during folliculogenesis.

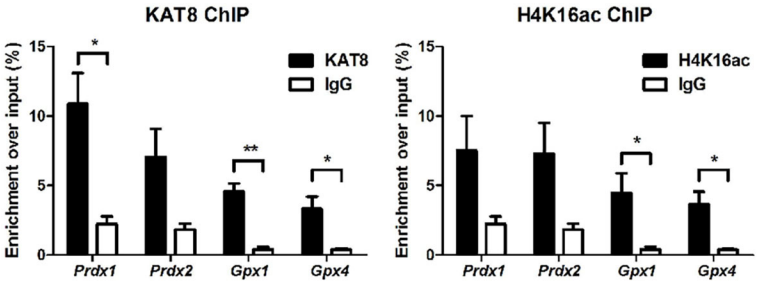

Fig. 7. KAT8 and H4K16ac levels at antioxidant gene promoters in oocytes. ChIP was performed using KAT8 or H4K16ac antibodies in oocytes from 2-week-old WT mice. Promoter regions of antioxidant genes were analyzed by real-time PCR. Data are expressed as the enrichment over the input. IgG was used as a negative control. **P*<0.05, ***P*<0.01, *t*-test. Data are mean±s.e.m. from three independent experiments.

Development (2017) 144, 2165-2174 doi:10.1242/dev.149518

Kat8 deletion results in abnormal heterochromatin configurations in oocytes

To examine the effect of *Kat8* deletion on heterochromatin, we immunostained for heterochromatin-associated protein HP1β (also known as CBX1) and for H3K9 trimethylation (H3K9me3) in $Kat8^{Gdf9}$ cKO oocytes. The majority (more than 80%) of heterochromatin regions in WT oocytes exhibited a normal oval or round shape, whereas more than 55% of heterochromatin regions in $Kat8^{Gdf9}$ cKO oocytes were irregularly shaped (Fig. S6), indicating that *Kat8* is essential for maintaining normal chromatin configurations in oocytes.

Granulosa cell-specific deletion of *Kat8* does not affect follicle development or female fertility

To identify the potential function of *Kat8* in granulosa cells, we generated mice in which *Kat8* was specifically deleted in granulosa cells by crossing female $Kat8^{flox/flox}$ mice with *Amhr2-Cre* males. *Amhr2-Cre;* $Kat8^{flox/flox}$ (referred to as $Kat8^{Amhr2}$ cKO) females exhibited negligible KAT8 protein levels in granulosa cells (Fig. S7A). However, $Kat8^{Amhr2}$ cKO females exhibited normal fertility and follicle development, similar to WT mice (Fig. S7B-D). These findings indicate that *Kat8* is dispensable in granulosa cells for female fertility.

DISCUSSION

Histone acetylation is important for the regulation of gene transcription and in many other cellular processes (Shahbazian and Grunstein, 2007). Here, we report that oocyte-specific deletion of *Kat8*, which encodes a HAT that controls the majority of H4K16 acetylation, results in a dramatic reduction in the number of secondary, preantral and antral follicles. *Kat8*-deficient oocytes have increased basal levels of DSBs and undergo apoptosis due to accumulation of ROS.

In oocytes, dramatic changes in gene expression occur during the transition from secondary follicle to small antral follicle (Pan et al., 2005), but the mechanisms regulating this transition are largely unknown. Here, we found that *Kat8* deletion in oocytes leads to abnormal gene expression (Fig. S5, Tables S3 and S4) and significantly reduces the number of secondary, preantral and antral follicles (Fig. 3A,B). These results confirm that *Kat8* is important for regulating gene expression in oocytes. Following *Kat8* deletion in oocytes, follicle development was accompanied by morphological abnormalities and increased oocyte apoptosis (Fig. 3C,D). Many factors, including ROS, have been reported to induce oocyte apoptosis (Tiwari et al., 2015). Indeed, increased ROS levels were observed in $Kat8^{Gdf9}$ cKO oocytes (Fig. 4B,C). Moreover, the ratio of apoptotic oocytes and the number of degenerating follicles per section were restored to near normal levels after NAC treatment for 7 days (Fig. 5F, Fig. 6E,F). These results not only confirm accumulation of ROS as the main cause for follicle degeneration in $Kat8^{Gdf9}$ cKO mice, but also indicate that KAT8 protects the normal development of oocytes and follicles by indirectly controlling ROS levels.

Increased ROS levels can cause abnormal cellular redox circuits and damage cellular macromolecules, such as DNA (Kim et al., 2012; Roberts et al., 2009). We detected increased levels of DSBs in *Kat8*-deficient oocytes. Our observation that treatment of $Kat8^{Gdf9}$ cKO oocytes with NAC, an antioxidant drug that can reduce ROS levels, significantly decreased DSB accumulation (Fig. 6A-D) indicates that ROS accumulation is the main cause of DNA damage in $Kat8^{Gdf9}$ cKO oocytes. Although reports have shown that KAT8 can directly contribute to DSB repair (Gupta et al., 2014; Sharma et al., 2010), data from our rescue experiment suggest that, in oocytes, KAT8 primarily prevents DSB generation by limiting ROS levels.

In most cells, including oocytes, ROS are removed by a series of antioxidant enzymes (Devine et al., 2012). RNA-seq and real-time PCR showed that in $Kat8^{Gdf9}$ cKO oocytes the antioxidant genes *Prdx1*, *Prdx2*, *Gpx1* and *Gpx4*, which encode components of ROS-scavenging systems (Brigelius-Flohé and Maiorino, 2013; Rhee, 2016), were significantly downregulated (Table S4, Fig. 4A). ChIP assays further established that KAT8 directly binds the promoters of *Prdx1*, *Gpx1* and *Gpx4*. Unexpectedly, although H4K16ac, the histone target of KAT8, is important for gene expression (Dion et al., 2005), ChIP results identified H4K16ac only at the *Gpx1* and *Gpx4* promoters. This indicates that KAT8 can directly regulate gene expression independently of H4K16 acetylation in mouse oocytes, which was also suggested by outcomes of a recent study in mouse ESCs (Taylor et al., 2013).

It should be noted that $Kat8^{Gdf9}$ cKO mice are sterile, whereas mice lacking *Gpx4* display embryonic lethality (Yant et al., 2003) and mice deficient for *Prdx1*, *Prdx2* or *Gpx1* are viable and fertile (Ho et al., 1997; Lee et al., 2003; Neumann et al., 2003). An explanation for this discrepancy is that the expression and/or functional loss may be compensated for by other Gpx and Prdx family members. For example, in the spleen of *Prdx1* knockout mice, *Gpx1* expression increases more than 2-fold (Rani et al., 2012). Silencing of *Prdx2* alone in hepatocellular carcinoma cells has no effect on cell survival, whereas simultaneous silencing of *Prdx1* and *Prdx2* promotes cell death (Hou et al., 2014). These studies indicate synergetic effects on cells of Gpx and Prdx factors, and suggest that the simultaneous reduction of *Prdx1*, *Prdx2*, *Gpx1* and *Gpx4* could be the reason for excessive apoptosis in $Kat8^{Gdf9}$ cKO oocytes.

Accumulation of ROS is a major cause of the defective oogenesis and follicle development in $Kat8^{Gdf9}$ cKO mice. However, treatment of $Kat8^{Gdf9}$ cKO mice with NAC did not entirely restore ovary size and oocyte and follicle numbers (Fig. 5). One explanation might be that oocyte apoptosis and follicle degeneration occurred before NAC administration/function. Other possibilities remain. For example, besides antioxidant genes, several oocyte-specific genes such as *Oosp1* and *Omt2b* (West et al., 1996; Yan et al., 2001) were also downregulated in $Kat8^{Gdf9}$ cKO oocytes (Fig. S5A, Table S4). Whether the misregulation of these genes contributes to the disrupted follicle development needs to be tested.

Our results show that H4K16ac levels increase during mouse oocyte development from 5 days to the GV stage, when transcription is becoming active (Lucifero et al., 2007), and then significantly decreases upon GVBD (Fig. S1), when the oocytes become transcriptionally silent and chromatin condensation starts (De La Fuente and Eppig, 2001; Kageyama et al., 2007). Mouse oocytes lacking H4K16ac due to *Kat8* deletion displayed abnormal gene expression (Fig. S5, Tables S3 and S4) and increased apoptosis before reaching the full-grown GV stage (Fig. 3C,D). Interestingly, increasing H4K16ac by repressing *Hdac2* or *Sirt6* expression results in a decreased number of antral follicles (Ma and Schultz, 2013), abnormal spindle assembly, and defective chromosome segregation in MII cells (Han et al., 2015; Ma and Schultz, 2013). These findings show that the temporal regulation of H4K16ac levels is crucial for oogenesis, with high levels required for gene expression and normal oocyte growth, and low levels essential for progression through meiosis II.

Although oocyte-granulosa cell communication is important for follicle development by regulating granulosa cell proliferation

Development (2017) 144, 2165-2174 doi:10.1242/dev.149518

(Su et al., 2009), *Gdf9* and *Bmp15*, which encode two important oocyte-derived factors responsible for granulosa cell proliferation (McNatty et al., 2005), were expressed at comparable levels in WT and *Kat8*^{Gdf9} cKO oocytes (Fig. S4C). Consistent with this, BrdU incorporation and PCNA immunostaining showed that the proliferation of granulosa cells in *Kat8*^{Gdf9} cKO ovaries remained normal (Fig. S4A,B). These results suggest that the oocyte-granulosa cell communication responsible for granulosa cell proliferation is not affected by *Kat8* deletion in oocytes.

In conclusion, our data show that the H4K16-specific HAT KAT8 promotes the expression of antioxidant genes in developing oocytes directly or by H4K16ac. These antioxidant proteins reduce ROS levels to prevent the generation of DSBs and to guarantee normal oocyte and follicle development. Our study demonstrates, for the first time, that KAT8 is essential for female fertility, and suggests that histone modifications, at least H4K16ac, should be considered in genetic counseling and when exploring the molecular basis of human ovarian folliculogenesis failure.

MATERIALS AND METHODS

Mice

Kat8$^{flox/flox}$ mice, which have loxP sites flanking exons 1 to 3 of *Kat8*, were described previously (Gupta et al., 2008; Kumar et al., 2011), *Gdf9-Cre* transgenic mice were purchased from The Jackson Laboratory and *Amhr2-Cre* knock-in mice were kindly donated by Dr. R. Behringer (Jamin et al., 2002). All the mice were maintained on a mixed C57BL/6 and SV129 genetic background. For fertility tests, 8- to 10-week-old WT, *Kat8*^{Gdf9} cKO and *Kat8*^{Amhr2} cKO females were separately housed with WT males for 6 months. The number of offspring from each pregnant female was recorded after birth. All animal experiments were performed according to the guidelines and procedures approved by the Institutional Animal Care Committee of the University of Science and Technology of China.

Oocyte and granulosa cell collection

Female mice (7-8 weeks old) were intraperitoneally injected with 5 IU PMSG (Ningbo Sansheng Pharmaceutical Corporation, Zhejiang, China). Forty-eight hours post injection, ovaries were collected and placed in M2 medium (Sigma, M7167) supplemented with 200 µM IBMX (Sigma, I7108) at 37°C to prevent GVBD. Full-grown GV oocytes and granulosa cells were released by puncturing antral follicles with a fine needle under the visual field of a dissecting microscope. GVBD-MI oocytes (absence of both GV and polar body) (Kim et al., 2015) were obtained after moving GV oocytes to IBMX-free M16 medium (Sigma, M7292) and culturing for 2-4 h (Ma and Viveiros, 2014). For MII oocyte collection, mice were injected with PMSG as above followed by intraperitoneal injection with 5 IU human chorionic gonadotropin (HCG; Ningbo Sansheng Pharmaceutical Corporation) 48 h later. MII oocytes were collected from the oviducts 16 h post HCG injection. Meiotically incompetent oocytes (20-30 µm diameter from 5-day mice, and 50-70 µm diameter from 2- and 3-week-old mice) were obtained as described previously (Svoboda et al., 2001).

RNA extraction, cDNA synthesis, RT-PCR and real-time PCR

Total RNA was extracted from oocytes of 2-week-old mice using the RNAprep Pure Micro Kit (DP420, Tiangen, Beijing, China), and cDNA synthesis was performed using the PrimeScript Reagent Kit (Takara, RR047A) according to the manufacturer's instructions. For RT-PCR, PCR reactions (30 µl) included: 3 µl 10×Easy Taq DNA Polymerase Buffer (AP111, Trans, Beijing, China), 2 µl 2.5 mM dNTPs (Trans, AD101), 1 µl 10 µM forward and reverse PCR primers, 2 µl cDNA and 2.5 U Easy Taq DNA polymerase (Trans, AP111). The PCR program consisted of 32 cycles of denaturing at 95°C for 20 s, annealing at 59°C for 30 s and extension at 72°C for 30 s. Real-time PCR was performed as previously described (Xu et al., 2011) and data were normalized against *Actb*. Quantification of the fold change in gene expression was determined by the comparative C_T method. PCR primers are listed in Table S1.

Immunofluorescence

Oocytes were fixed in 4% paraformaldehyde (PFA) for 20 min at room temperature, followed by permeabilization in PBS containing 0.2% Triton X-100 for 15 min. After blocking with PBS containing 5% normal donkey serum (Jackson ImmunoResearch, 017-000-121) for 30 min, oocytes were incubated with primary antibodies at 37°C for 2 h, followed by incubation with secondary antibodies for 1 h at room temperature. After staining with Hoechst 33342 (Invitrogen, H21492), oocytes were transferred to slides and mounted using Vectashield (Vector Laboratories, H-1000). Fluorescence was detected on an Eclipse 80i microscope (Nikon) equipped with a digital camera (Hamamatsu, C4742-80). Antibodies are listed in Table S2.

Western blot analysis

Oocyte and granulosa cell lysates were prepared in lysis buffer (100 mM Tris-HCl pH 7.4, 3% SDS, 10 mM DTT, 17.3% glycerin, 0.15% Bromophenol Blue) supplemented with cOmplete Protease Inhibitor Cocktail (Roche, 04693116001). Western blot was performed as described previously (Wang et al., 2014) using the antibodies listed in Table S2.

Histological analysis

Ovaries were fixed in 4% PFA for 12-24 h before paraffin embedding, and 5 µm paraffin sections were attached to microscope slides for PAS-Hematoxylin or Hematoxylin staining. Samples were analyzed using an Eclipse 80i microscope equipped with a DS-Ri1 digital camera (Nikon).

TUNEL assay

TUNEL assay was performed in oocytes and ovary paraffin sections according to the instructions provided with the In Situ Cell Death Detection Kit (Roche, 11684795910). Fluorescence was detected using the Nikon Eclipse 80i microscope and Hamamatsu digital camera (C4742-80).

BrdU incorporation

Two-week-old mice were intraperitoneally injected with BrdU (100 mg/kg; Sigma, B9285) and were sacrificed 2 h post injection. Ovary sections were immunostained using an anti-BrdU antibody and analyzed using the Eclipse 80i microscope and DS-Ri1 camera. Antibodies used are listed in Table S2.

PCNA immunostaining

Ovary sections from 2-week-old mice were immunostained using anti-PCNA antibody (Table S2) and analyzed using the Eclipse 80i microscope and DS-Ri1 camera.

RNA-seq analysis

RNA-seq was conducted by Shanghai Biotechnology Corporation. Briefly, each sample, which contained ~300 oocytes collected from eight 2-week-old WT and *Kat8*^{Gdf9} cKO mice, was lysed directly in 3.5 µl RNase-free water supplemented with 0.2% Triton X-100 and 7 U RiboLock RNase Inhibitor (Thermo, EO0381) and immediately stored at −80°C until use. RNA was amplified using the SMARTer Ultra Low Input RNA Kit (Clontech, 634823), the resulting cDNA fragmented using a Covaris S2 ultrasonicator, and paired-end libraries constructed using the Ovation Ultralow DR Multiplex System 1-96 (NuGEN Technologies, 0329-96). The libraries were sequenced on an Illumina HiSeq 2500 instrument (SY-401-2501), generating 54-63 million pairs of reads per sample. Each pair of reads represents a cDNA fragment from the library. The reads were mapped to the mouse reference genome (mm10) using TopHat (version 2.0.9) (Trapnell et al., 2009). Differential gene expression between WT and *Kat8*^{Gdf9} cKO oocytes was determined using Cufflinks (version 2.1.1) (Zhang et al., 2015). The threshold for significance was a false discovery rate ≤0.05 and a fold expression change ≥2. GO analysis was performed using Ingenuity Pathway Analysis (IPA) software. Processed RNA-seq data are presented in Tables S3 and S4 and the full data set has been deposited in the GEO database (accession GSE97026).

Oxidative stress assessment

ROS levels were assessed using carboxy-H2DCFDA (s0033, Beyotime, Jiangsu, China). Briefly, oocytes from 2- or 3-week-old mice were incubated in M2 medium containing 10 µM carboxy-H2DCFDA at 37°C

Development (2017) 144, 2165-2174 doi:10.1242/dev.149518

for 20 min, followed by staining with Hoechst 33342. Fluorescence was detected on a Nikon TE2000E microscope equipped with a Nikon DS-Qi1Mc digital camera. Fluorescence intensity was quantified using ImageJ software (National Institutes of Health).

ChIP and real-time PCR

ChIP was performed using the Pierce Agarose ChIP Kit (Thermo, 26156) according to the manufacturer's instructions. In brief, ∼3000 oocytes from 2-week-old mice were cross-linked in 4% formaldehyde at room temperature for 15 min. Fixation was stopped by addition of 10×Glycine Solution. Oocytes were then incubated at room temperature for 5 min, washed in ice-cold PBS containing 1% Halt Cocktail, and immediately stored at −80°C before lysis. Following enzyme-mediated nuclear lysis, samples were sonicated for 1 min to completely fragment the chromatin. Promoter region primers spanning −700 to +300 bp relative to the gene transcription start sites were used, and gene enrichment was quantified by real-time PCR. PCR primers and antibodies used are listed in Tables S1 and S2.

N-acetylcysteine treatment

Two-week-old mice were injected intraperitoneally with NAC (150 mg/kg; Beyotime, s0077) or PBS once per day for 7 days. The NAC dose of 150 mg/kg was based on the studies by Mahmoodi et al. (2015). Ovaries were then collected for histological analysis and oocytes isolated for ROS detection, γ-H2AX staining and TUNEL assay.

Statistical analysis

Statistical comparison was performed using Student's unpaired two-tailed *t*-test, one-way ANOVA (Tukey's multiple comparison test) or Chi-square test. All experiments were performed at least three times and results are presented as mean±s.e.m. Statistical significance was set at $P<0.05$.

Acknowledgements

We are very thankful to Dr R. Behringer for donation of the *Amhr2-Cre* mice and S. Eckardt for help with manuscript modification.

Competing interests

The authors declare no competing or financial interests.

Author contributions

Conceptualization: S.Y., Q.S.; Methodology: X.J., S.Y., Q.G., Y.Z.; Software: Y.Z.; Validation: S.Y., S.F.; Investigation: S.Y., Q.G.; Resources: H.J., T.K.P., H.-Y.F.; Writing - original draft: X.J., S.Y.; Writing - review & editing: X.J., F.W., T.K., N.J., M.K., A.A., P.X., T.K.P., Q.S.; Supervision: Q.S.; Funding acquisition: X.J., Q.S. F.W., T.K.P.

Funding

This work was supported by the National Health and Family Planning Commission of the People's Republic of China (2016YFC1000600), Ministry of Science and Technology of the People's Republic of China (2013CB945502), the Strategic Priority Research Program of the Chinese Academy of Sciences (XDB19000000), the National Natural Science Foundation of China (31501199, 31671557, 31501203 and 31371519), the National Natural Science Foundation of China - Israel Science Foundation (31461143013-1183/14), Major Program of Development Foundation of Hefei Institutes of Physical Science, Chinese Academy of Sciences (2014FXZY003), the Fundamental Research Funds for the Central Universities (WK2340000069), and the National Institutes of Health (RO1 CA129537, RO1 GM109768). Deposited in PMC for release after 12 months.

Data availability

RNA-seq data have been deposited at Gene Expression Omnibus under accession number GSE97026.

Supplementary information

Supplementary information available online at
http://dev.biologists.org/lookup/doi/10.1242/dev.149518.supplemental

References

Akhtar, A. and Becker, P. B. (2000). Activation of transcription through histone H4 acetylation by MOF, an acetyltransferase essential for dosage compensation in Drosophila. *Mol. Cell* **5**, 367-375.

Brigelius-Flohé, R. and Maiorino, M. (2013). Glutathione peroxidases. *Biochim. Biophys. Acta* **1830**, 3289-3303.

Danilovic, A., Lucon, A. M., Srougi, M., Shimizu, M. H. M., Ianhez, L. E., Nahas, W. C. and Seguro, A. C. (2011). Protective effect of N-acetylcysteine on early outcomes of deceased renal transplantation. *Transplant. Proc.* **43**, 1443-1449.

De La Fuente, R. and Eppig, J. J. (2001). Transcriptional activity of the mouse oocyte genome: companion granulosa cells modulate transcription and chromatin remodeling. *Dev. Biol.* **229**, 224-236.

Devine, P. J., Perreault, S. D. and Luderer, U. (2012). Roles of reactive oxygen species and antioxidants in ovarian toxicity. *Biol. Reprod.* **86**, 27.

Dion, M. F., Altschuler, S. J., Wu, L. F. and Rando, O. J. (2005). Genomic characterization reveals a simple histone H4 acetylation code. *Proc. Natl. Acad. Sci. USA* **102**, 5501-5506.

Gu, L., Wang, Q. and Sun, Q.-Y. (2010). Histone modifications during mammalian oocyte maturation: dynamics, regulation and functions. *Cell Cycle* **9**, 1942-1950.

Gupta, A., Guerin-Peyrou, T. G., Sharma, G. G., Park, C., Agarwal, M., Ganju, R. K., Pandita, S., Choi, K., Sukumar, S., Pandita, R. K. et al. (2008). The mammalian ortholog of Drosophila MOF that acetylates histone H4 lysine 16 is essential for embryogenesis and oncogenesis. *Mol. Cell. Biol.* **28**, 397-409.

Gupta, A., Hunt, C. R., Pandita, R. K., Pae, J., Komal, K., Singh, M., Shay, J. W., Kumar, R., Ariizumi, K., Horikoshi, N. et al. (2013). T-cell-specific deletion of Mof blocks their differentiation and results in genomic instability in mice. *Mutagenesis* **28**, 263-270.

Gupta, A., Hunt, C. R., Hegde, M. L., Chakraborty, S., Chakraborty, S., Udayakumar, D., Horikoshi, N., Singh, M., Ramnarain, D. B., Hittelman, W. N. et al. (2014). MOF phosphorylation by ATM regulates 53BP1-mediated double-strand break repair pathway choice. *Cell Rep.* **8**, 177-189.

Han, L., Ge, J., Zhang, L., Ma, R., Hou, X., Li, B., Moley, K. and Wang, Q. (2015). Sirt6 depletion causes spindle defects and chromosome misalignment during meiosis of mouse oocyte. *Sci. Rep.* **5**, 15366.

Ho, Y.-S., Magnenat, J.-L., Bronson, R. T., Cao, J., Gargano, M., Sugawara, M. and Funk, C. D. (1997). Mice deficient in cellular glutathione peroxidase develop normally and show no increased sensitivity to hyperoxia. *J. Biol. Chem.* **272**, 16644-16651.

Hou, J.-K., Huang, Y., He, W., Yan, Z.-W., Fan, L., Liu, M.-H., Xiao, W.-L., Sun, H.-D. and Chen, G.-Q. (2014). Adenanthin targets peroxiredoxin I/II to kill hepatocellular carcinoma cells. *Cell Death Dis.* **5**, e1400.

Inci, I., Zhai, W., Arni, S., Hillinger, S., Vogt, P. and Weder, W. (2007). N-acetylcysteine attenuates lung ischemia-reperfusion injury after lung transplantation. *Ann. Thorac. Surg.* **84**, 240-246.

Jagarlamudi, K. and Rajkovic, A. (2012). Oogenesis: transcriptional regulators and mouse models. *Mol. Cell. Endocrinol.* **356**, 31-39.

Jamin, S. P., Arango, N. A., Mishina, Y., Hanks, M. C. and Behringer, R. R. (2002). Requirement of Bmpr1a for Müllerian duct regression during male sexual development. *Nat. Genet.* **32**, 408-410.

Kageyama, S.-I., Liu, H., Kaneko, N., Ooga, M., Nagata, M. and Aoki, F. (2007). Alterations in epigenetic modifications during oocyte growth in mice. *Reproduction* **133**, 85-94.

Kim, S. B., Pandita, R. K., Eskiocak, U., Ly, P., Kaisani, A., Kumar, R., Cornelius, C., Wright, W. E., Pandita, T. K. and Shay, J. W. (2012). Targeting of Nrf2 induces DNA damage signaling and protects colonic epithelial cells from ionizing radiation. *Proc. Natl. Acad. Sci. USA* **109**, E2949-E2955.

Kim, J., Singh, A. K., Takata, Y., Lin, K., Shen, J., Lu, Y., Kerenyi, M. A., Orkin, S. H. and Chen, T. (2015). LSD1 is essential for oocyte meiotic progression by regulating CDC25B expression in mice. *Nat. Commun.* **6**, 10116.

Kumar, R., Hunt, C. R., Gupta, A., Nannepaga, S., Pandita, R. K., Shay, J. W., Bachoo, R., Ludwig, T., Burns, D. K. and Pandita, T. K. (2011). Purkinje cell-specific males absent on the first (mMof) gene deletion results in an ataxia-telangiectasia-like neurological phenotype and backward walking in mice. *Proc. Natl. Acad. Sci. USA* **108**, 3636-3641.

Lan, Z.-J., Xu, X. and Cooney, A. J. (2004). Differential oocyte-specific expression of Cre recombinase activity in GDF-9-iCre, Zp3cre, and Msx2Cre transgenic mice. *Biol. Reprod.* **71**, 1469-1474.

Lee, T.-H., Kim, S. U., Yu, S. L., Kim, S. H., Park, D. S., Moon, H. B., Dho, S. H., Kwon, K. S., Kwon, H. J., Han, Y. H. et al. (2003). Peroxiredoxin II is essential for sustaining life span of erythrocytes in mice. *Blood* **101**, 5033-5038.

Li, X., Li, L., Pandey, R., Byun, J. S., Gardner, K., Qin, Z. and Dou, Y. (2012). The histone acetyltransferase MOF is a key regulator of the embryonic stem cell core transcriptional network. *Cell Stem Cell* **11**, 163-178.

Lucifero, D., La Salle, S., Bourc'his, D., Martel, J., Bestor, T. H. and Trasler, J. M. (2007). Coordinate regulation of DNA methyltransferase expression during oogenesis. *BMC Dev. Biol.* **7**, 36.

Ma, P. and Schultz, R. M. (2013). Histone deacetylase 2 (HDAC2) regulates chromosome segregation and kinetochore function via H4K16 deacetylation during oocyte maturation in mouse. *PLoS Genet.* **9**, e1003377.

Ma, W. and Viveiros, M. M. (2014). Depletion of pericentrin in mouse oocytes disrupts microtubule organizing center function and meiotic spindle organization. *Mol. Reprod. Dev.* **81**, 1019-1029.

Ma, P., Pan, H., Montgomery, R. L., Olson, E. N. and Schultz, R. M. (2012). Compensatory functions of histone deacetylase 1 (HDAC1) and HDAC2 regulate transcription and apoptosis during mouse oocyte development. *Proc. Natl. Acad. Sci. USA* **109**, E481-E489.

Ma, J.-Y., Ou-Yang, Y.-C., Wang, Z.-W., Wang, Z., Jiang, Z.-Z., Luo, S.-M., Hou, Y., Liu, Z., Schatten, H. and Sun, Q.-Y. (2013). The effects of DNA double-strand breaks on mouse oocyte meiotic maturation. *Cell Cycle* **12**, 1233-1241.

Mahmoodi, M., Soleimani Mehranjani, M., Shariatzadeh, S. M. A., Eimani, H. and Shahverdi, A. (2015). N-acetylcysteine improves function and follicular survival in mice ovarian grafts through inhibition of oxidative stress. *Reprod. Biomed. Online* **30**, 101-110.

McNatty, K. P., Juengel, J. L., Reader, K. L., Lun, S., Myllymaa, S., Lawrence, S. B., Western, A., Meerasahib, M. F., Mottershead, D. G., Groome, N. P. et al. (2005). Bone morphogenetic protein 15 and growth differentiation factor 9 co-operate to regulate granulosa cell function in ruminants. *Reproduction* **129**, 481-487.

Monti, M. and Redi, C. A. (2009). Oogenesis specific genes (Nobox, Oct4, Bmp15, Gdf9, Oogenesin1 and Oogenesin2) are differentially expressed during natural and gonadotropin-induced mouse follicular development. *Mol. Reprod. Dev.* **76**, 994-1003.

Neumann, C. A., Krause, D. S., Carman, C. V., Das, S., Dubey, D. P., Abraham, J. L., Bronson, R. T., Fujiwara, Y., Orkin, S. H. and Van Etten, R. A. (2003). Essential role for the peroxiredoxin Prdx1 in erythrocyte antioxidant defence and tumour suppression. *Nature* **424**, 561-565.

Pan, H., O'Brien, M. J., Wigglesworth, K., Eppig, J. J. and Schultz, R. M. (2005). Transcript profiling during mouse oocyte development and the effect of gonadotropin priming and development in vitro. *Dev. Biol.* **286**, 493-506.

Pan, Z., Zhang, J., Li, Q., Li, Y., Shi, F., Xie, Z. and Liu, H. (2012). Current advances in epigenetic modification and alteration during mammalian ovarian folliculogenesis. *J. Genet. Genomics* **39**, 111-123.

Rani, V., Neumann, C. A., Shao, C. and Tischfield, J. A. (2012). Prdx1 deficiency in mice promotes tissue specific loss of heterozygosity mediated by deficiency in DNA repair and increased oxidative stress. *Mutat. Res.* **735**, 39-45.

Rhee, S. G. (2016). Overview on Peroxiredoxin. *Mol. Cells* **39**, 1-5.

Roberts, R. A., Laskin, D. L., Smith, C. V., Robertson, F. M., Allen, E. M. G., Doorn, J. A. and Slikker, W. (2009). Nitrative and oxidative stress in toxicology and disease. *Toxicol. Sci.* **112**, 4-16.

Rodrigues, P., Limback, D., McGinnis, L. K., Plancha, C. E. and Albertini, D. F. (2008). Oogenesis: prospects and challenges for the future. *J. Cell. Physiol.* **216**, 355-365.

Shahbazian, M. D. and Grunstein, M. (2007). Functions of site-specific histone acetylation and deacetylation. *Annu. Rev. Biochem.* **76**, 75-100.

Sharma, G. G., So, S., Gupta, A., Kumar, R., Cayrou, C., Avvakumov, N., Bhadra, U., Pandita, R. K., Porteus, M. H., Chen, D. J. et al. (2010). MOF and histone H4 acetylation at lysine 16 are critical for DNA damage response and double-strand break repair. *Mol. Cell. Biol.* **30**, 3582-3595.

Su, Y.-Q., Sugiura, K. and Eppig, J. J. (2009). Mouse oocyte control of granulosa cell development and function: paracrine regulation of cumulus cell metabolism. *Semin. Reprod. Med.* **27**, 32-42.

Su, J., Wang, F., Cai, Y. and Jin, J. (2016). The functional analysis of histone acetyltransferase MOF in tumorigenesis. *Int. J. Mol. Sci.* **17**, 99.

Svoboda, P., Stein, P. and Schultz, R. M. (2001). RNAi in mouse oocytes and preimplantation embryos: effectiveness of hairpin dsRNA. *Biochem. Biophys. Res. Commun.* **287**, 1099-1104.

Taylor, G. C. A., Eskeland, R., Hekimoglu-Balkan, B., Pradeepa, M. M. and Bickmore, W. A. (2013). H4K16 acetylation marks active genes and enhancers of embryonic stem cells, but does not alter chromatin compaction. *Genome Res.* **23**, 2053-2065.

Thomas, T., Loveland, K. L. and Voss, A. K. (2007). The genes coding for the MYST family histone acetyltransferases, Tip60 and Mof, are expressed at high levels during sperm development. *Gene Expr. Patterns* **7**, 657-665.

Tiwari, M., Prasad, S., Tripathi, A., Pandey, A. N., Ali, I., Singh, A. K., Shrivastav, T. G. and Chaube, S. K. (2015). Apoptosis in mammalian oocytes: a review. *Apoptosis* **20**, 1019-1025.

Trapnell, C., Pachter, L. and Salzberg, S. L. (2009). TopHat: discovering splice junctions with RNA-Seq. *Bioinformatics* **25**, 1105-1111.

Usta, U., Inan, M., Erbas, H., Aydogdu, N., Oz Puyan, F. and Altaner, S. (2008). Tissue damage in rat ovaries subjected to torsion and detorsion: effects of L-carnitine and N-acetyl cysteine. *Pediatr. Surg. Int.* **24**, 567-573.

van den Hurk, R. and Zhao, J. (2005). Formation of mammalian oocytes and their growth, differentiation and maturation within ovarian follicles. *Theriogenology* **63**, 1717-1751.

Wang, Z., Yin, H., Zhang, Y., Feng, Y., Yan, Z., Jiang, X., Bukhari, I., Iqbal, F., Cooke, H. J. and Shi, Q. (2014). miR-214-mediated downregulation of RNF8 induces chromosomal instability in ovarian cancer cells. *Cell Cycle* **13**, 3519-3528.

West, M. F., Verrotti, A. C., Sallés, F. J., Tsirka, S. E. and Strickland, S. (1996). Isolation and characterization of two novel, cytoplasmically polyadenylated, oocyte-specific, mouse maternal RNAs. *Dev. Biol.* **175**, 132-141.

Xu, B., Hua, J., Zhang, Y., Jiang, X., Zhang, H., Ma, T., Zheng, W., Sun, R., Shen, W., Sha, J. et al. (2011). Proliferating cell nuclear antigen (PCNA) regulates primordial follicle assembly by promoting apoptosis of oocytes in fetal and neonatal mouse ovaries. *PLoS ONE* **6**, e16046.

Yan, C., Pendola, F. L., Jacob, R., Lau, A. L., Eppig, J. J. and Matzuk, M. M. (2001). Oosp1 encodes a novel mouse oocyte-secreted protein. *Genesis* **31**, 105-110.

Yant, L. J., Ran, Q., Rao, L., Van Remmen, H., Shibatani, T., Belter, J. G., Motta, L., Richardson, A. and Prolla, T. A. (2003). The selenoprotein GPX4 is essential for mouse development and protects from radiation and oxidative damage insults. *Free Radic. Biol. Med.* **34**, 496-502.

Zhang, Y., Li, W., Dou, Y., Zhang, J., Jiang, G., Miao, L., Han, G., Liu, Y., Li, H. and Zhang, Z. (2015). Transcript quantification by RNA-Seq reveals differentially expressed genes in the red and yellow fruits of Fragaria vesca. *PLoS ONE* **10**, e0144356.

Supplementary Information

Supplementary Figures

Fig.S1

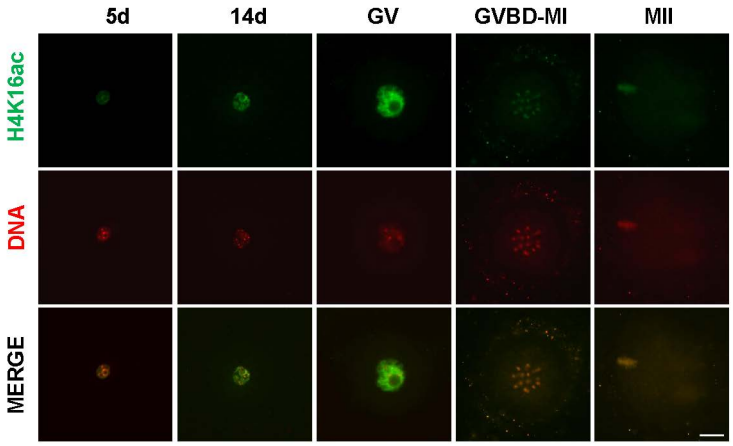

Fig.S1. H4K16ac levels in oocytes at different growth stages. Images shown are representative of three independent experiments. Scale bar: 20 μm.

Fig.S2

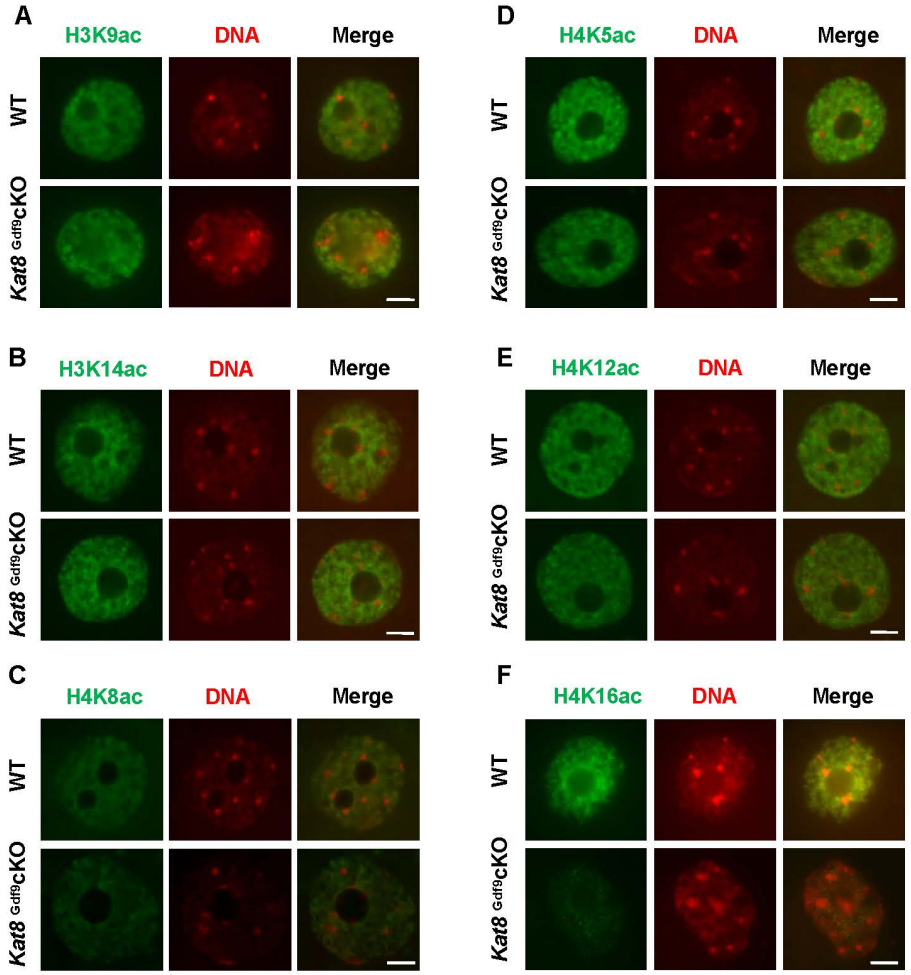

Fig.S2. *Kat8* deletion decreases H4K16ac level in oocytes. (A-F) Immunohistochemical analysis of histone modifications in oocytes from 2-week-old mice. Images are representative of three independent experiments and only the nuclei are shown. Scale bars: 10 μm.

Fig.S3

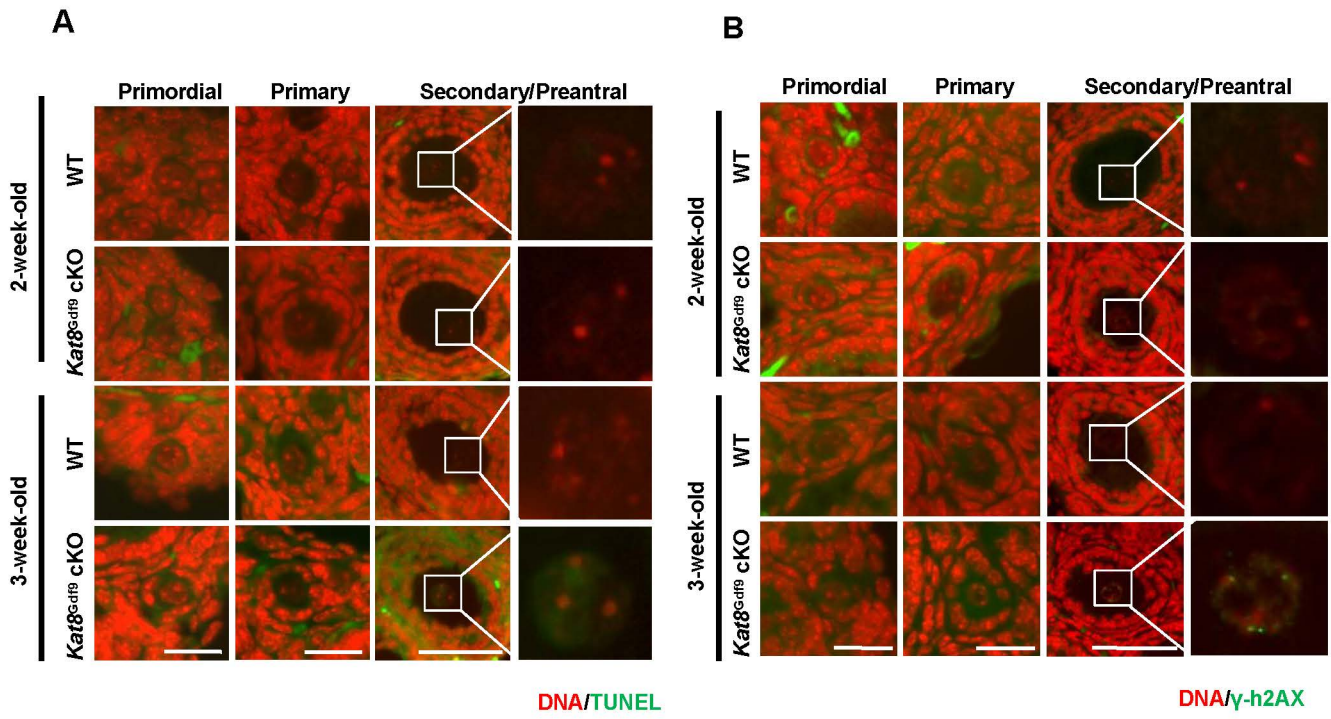

Fig.S3. Oocytes in growing follicles from 3-week-old *Kat8*^{Gdf9} cKO mice undergo apoptosis and exhibit severe DNA damage. (A) Apoptosis in oocytes at different stages of follicular development. TUNEL assay was performed in paraffin sections of ovaries from 2- and 3-week-old female mice. (B) Detection of DSBs in oocytes localized at different stages of follicular development by γ-H2AX staining in paraffin sections of ovaries from 2- and 3-week-old female mice. Images shown in A and B are representative of three independent experiments. Scale bars: for primordial and primary follicles, 20 μm; for secondary/preantral follicles, 50 μm.

Fig. S4

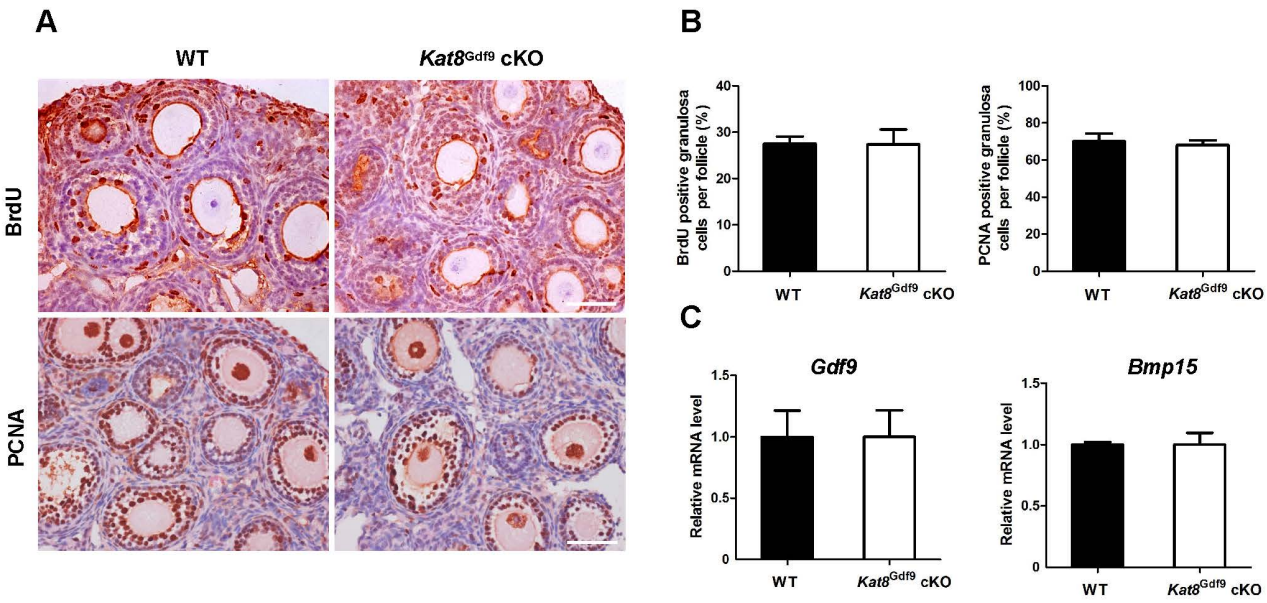

Fig.S4. Granulosa cell proliferation is unaffected in *Kat8*^{Gdf9} cKO females. (A) Immunostaining for the cell proliferation markers BrdU and PCNA in ovarian sections from 2-week-old mice. Images shown are representative of three independent experiments. Scale bars: 50 μm. (B) Percentage of BrdU and PCNA positive granulosa cells in secondary and preantral follicles shown in A. (C) Relative mRNA levels of *Gdf9* and *Bmp15* in oocytes from 2-week-old female mice detected by real-time PCR. Data shown in B and C are expressed as mean ± SEM from three independent experiments.

Fig.S5

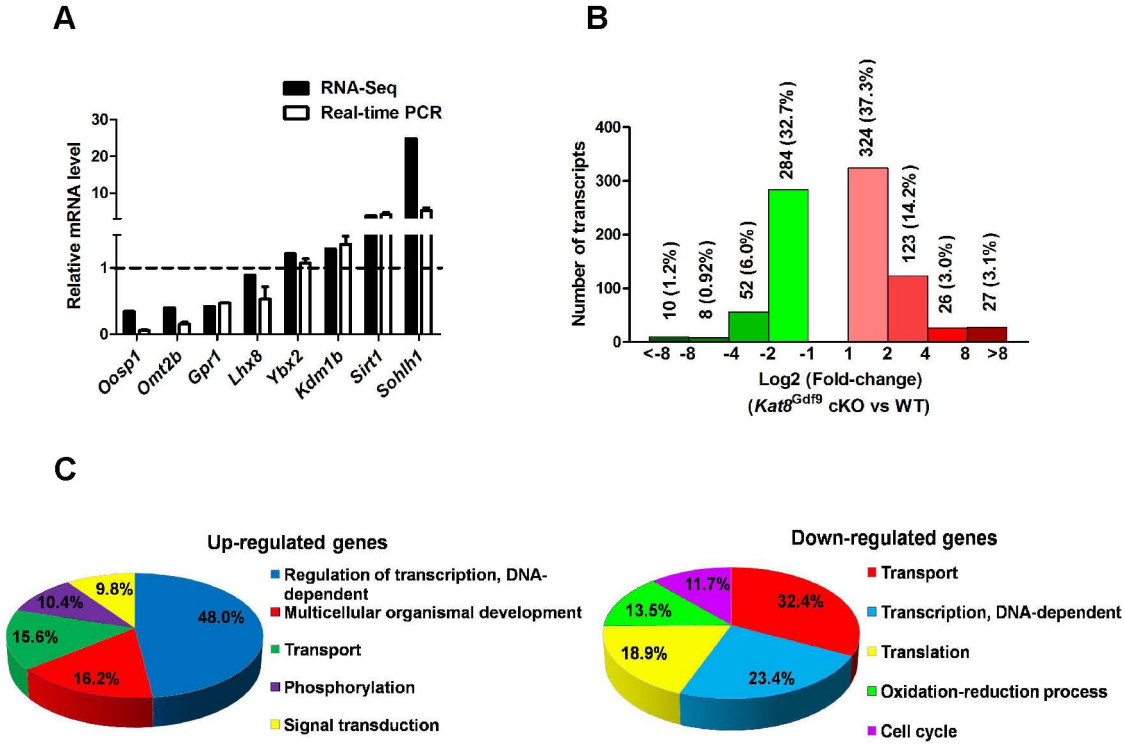

Fig.S5. Transcriptional profiling by RNA-seq. (A) Validation of RNA-seq data. Genes were selected from the RNA-seq data randomly and the expression levels were analyzed by real-time PCR in oocytes from 2-week-old mice. The mRNA levels detected by real-time PCR were normalized and plotted against *Actb*, and those in WT subsets were arbitrarily set to 1 (dotted line). (B) Distribution of differentially expressed genes at various magnitudes between WT and *Kat8*^{Gdf9} cKO oocytes by RNA-seq analysis. The number and ratio of each group genes are showed in the graph. (C) GO term analyses show the most enriched functional categories for the up- and down-regulated genes after *Kat8* deletion.

Fig.S6

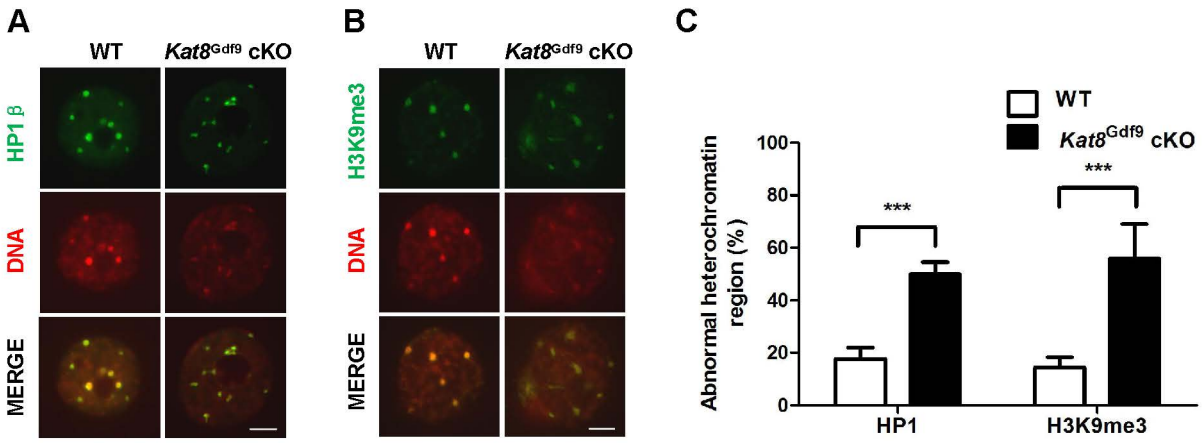

Fig.S6. *Kat8*^{Gdf9} cKO oocytes display abnormal heterochromatin configuration. (A) Immunostaining of heterochromatin-associated proteins HP1β and H3K9me3 in oocytes from 2-week-old mice. Images shown are representative of three independent experiments. Scale bar: 10 μm. (B) Percentages of heterochromatin regions with abnormal configuration to total heterochromatin regions. $^{**}P < 0.01$, $^{***}P < 0.001$, *t*-test. Data shown are expressed as mean ± SEM from three independent experiments.

Fig.S7

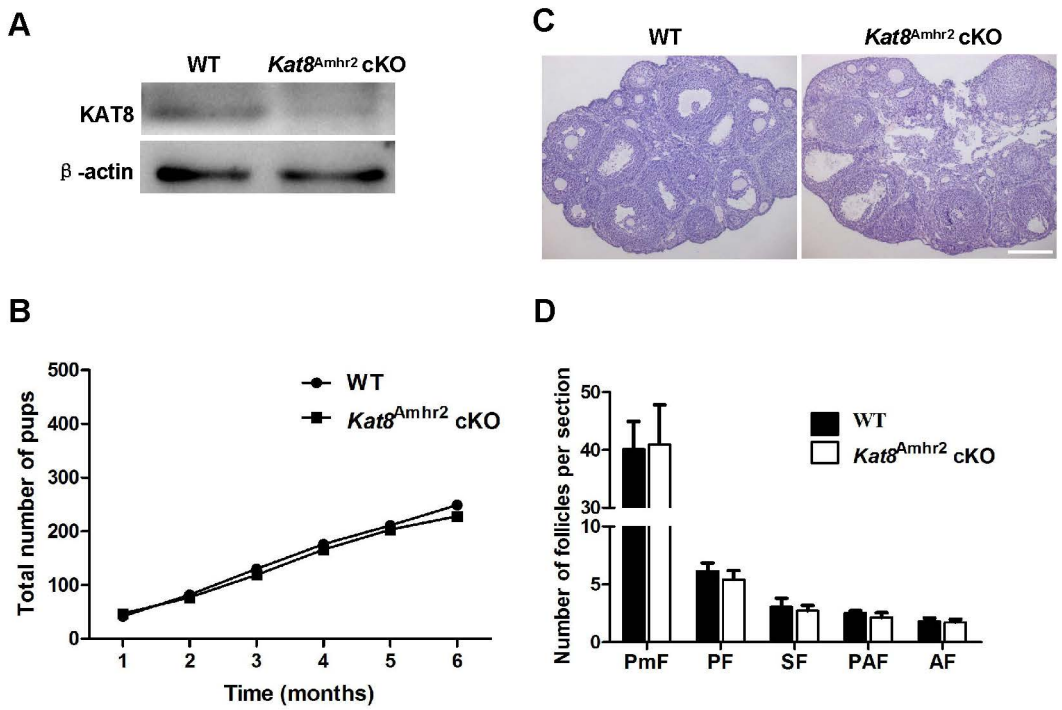

Fig.S7. *Kat8* deletion in granulosa cells has no effects on folliculogenesis and fertility. (A) Granulosa cells from 6-week-old WT and *Kat8*^{Amhr2} cKO mice were collected for Western blot analysis of KAT8. β-actin was served as a protein loading control. (B) Fertility test. The cumulative number of pups from 7 WT and 7 *Kat8*^{Amhr2} cKO females over a 6-month period is shown. (C) Haematoxylin staining of the ovarian sections from 6-week-old mice. Scale bar: 200 μm. (D) Follicles at different stages were quantified in ovarian sections from 6-week-old old mice. Data shown are expressed as mean ± SEM from three independent experiments. Images shown in A and C are representative of three independent experiments.

Supplementary Tables

Table S1. PCR Primers

Primers	Sequences (5' – 3')	Applications
Kat8 F	CTGGAAGGGCCAGCATGTTA	RT-PCR;Real-time PCR
Kat8 R	GGTTAGAGGCCAGGAAACCC	RT-PCR;Real-time PCR
Actb F	GCGTGACATCAAAGAGAAGC	RT-PCR;Real-time PCR
Actb R	AGGATTCCATACCCAAGAAGG	RT-PCR;Real-time PCR
Gdf9 F	ATGGGACAACTGGATCGTGG	Real-time PCR
Gdf9 R	CACTCAGGGGGCTGTACTTG	Real-time PCR
Bmp15 F	AGCACAGCATGGTTTCCCTT	Real-time PCR
Bmp15 R	GGGGGTATTCCATGTCTCACAC	Real-time PCR
Prdx1 F	GCACTGGACCATTTTTCTGCC	Real-time PCR
Prdx1 R	GATTGGTCTGCCCAAAACACAG	Real-time PCR
Prdx2 F	TGGGCCCAGGTCTATAGGAAA	Real-time PCR
Prdx2 R	TTGGTCTCACTGTGTCCCAC	Real-time PCR
Gpx1 F	CCGCTTTCGTACCATCGACA	Real-time PCR
Gpx1 R	CGCCCATCTGAGGGGATTTT	Real-time PCR
Gpx4 F	TGGATGAAAGTCCAGCCCAAG	Real-time PCR
Gpx4 R	GTGTAGGGGCACACACTTGTA	Real-time PCR
Oosp1 F	GGACTTACTCCTGCGGCATT	Real-time PCR
Oosp1 R	TCCATCCAGGAGGATCACCA	Real-time PCR
Omt2b F	TTTGAGGCCGGAACTATTGCT	Real-time PCR
Omt2b R	CCAGGCTCTGGCTCGATTT	Real-time PCR
Gpr1 F	TGCTGCAGACGTGGTAATGT	Real-time PCR
Gpr1 R	TGGTGAAGATCTATGCAGGCTC	Real-time PCR
Ybx2 F	CTCAGGTGGGACAGAACCTG	Real-time PCR
Ybx2 R	ATCACCCTCCAATGGTGCTG	Real-time PCR
Lhx8 F	AAGGCAGGACTGATCGTGTG	Real-time PCR
Lhx8 R	GCTTGTCCCGAAAACACTGG	Real-time PCR
Sirt1 F	TGCTGCAGACGTGGTAATGT	Real-time PCR
Sirt1 R	TGGTGAAGATCTATGCAGGCTC	Real-time PCR
Kdm1b F	CTCTTCTCCCCTGTCAAAGTACAA	Real-time PCR
Kdm1b R	GGGCCATTTAACATTGTGCACTTA	Real-time PCR
Sohlh1 F	GAGCCAAGCTTCATCGGAGA	Real-time PCR
Sohlh1 R	ACAGCTCCCCAGCAAACTAAA	Real-time PCR
*Prdx*1 ChIP F	TGCGTTCTCACGGCTCTTT	ChIP
Prdx1 ChIP R	GAGTAGAGCTCCAGCACTCG	ChIP
Prdx2 ChIP F	AGCCGCAATGGATCCGAC	ChIP
Prdx2 ChIP R	TGGGTTTTCATACCTGCGTGA	ChIP
Gpx1 ChIP F	ACAATATAAGGGAGCTGTGCGT	ChIP
Gpx1 ChIP R	CTAGGGCGGGTCTGGTCTA	ChIP
Gpx4 ChIP F	CTCCTGTACTTTCAAAGGGGCT	ChIP
Gpx4 ChIP R	GATAGGGACGCGGGAGAAAC	ChIP

Table S2. Antibodies

Antibodies	Vendors; Cat. No.	Dilution	Applications
KAT8	LifeSpan BioSciences, LS-C287822	1:100	Western Blot
		1:100	Immunofluorescence;
		1:250	ChIP
H4K16ac	Millipore; 07-329	1:100	Western Blot
		1:200	Immunofluorescence
		1:250	ChIP
IgG	Thermol; 26156	1:250	ChIP
β-actin	Abcam; ab8227	1:500	Western Blot
IgG	Cell signalling; 2729S	1:100	Immunofluorescence
γ-H2AX	Calbiochem; DR1017	1:15000	Immunofluorescence
BrdU	Molecular Probes; A21300	1:200	Immunohistochemistry
PCNA	Santa Cruz; SC-56	1:200	Immunohistochemistry
Secondary anti-mouse biotinylated antibody	Maixin; Bio, KIT-5010	1:1000	Immunohistochemistry
H3K9ac	Abcam; ab10812	1:200	Immunofluorescence
H3K14ac	Immunoway; YK0007	1:200	Immunofluorescence
H4K5ac	Immunoway; YK0011	1:200	Immunofluorescence
H4K8ac	Immunoway; YK0012	1:200	Immunofluorescence
H4K12ac	Immunoway; YK0013	1:200	Immunofluorescence
HP1 β	Abcam; ab10478	1:200	Immunofluorescence
H3K9me3	Abclonal; A2360	1:200	Immunofluorescence
Donkey Anti-Rabbit IgG(H+L) (Alexa Fluor 555)	Molecular Probes; A31572	1:250	Immunofluorescence
Donkey polyclonal Secondary Antibody to Rabbit IgG-H&L (HRP)	Abcam; ab6802	1:500	Western Blot

Table S3. Genes upregulated in *Kat8* Gdf9 cKO compared with WT oocytes.

Click here to Download Table S3

Table S4. Genes downregulated in *Kat8* Gdf9 cKO compared with WT oocytes.

Click here to Download Table S4